

Branch Growth and Sidebranching in Snow Crystals

Jon Nelson*

Sci-cubed 43812 SE 143rd Street, North Bend, Washington 98045

Received September 19, 2004; Revised Manuscript Received March 17, 2005

ABSTRACT: Why do some snow crystals have branches with many sidebranches, whereas other crystals have no sidebranches? To answer this question and gain an understanding of other common features of snow crystal branches, a macrostep model of branch growth is proposed. This model is developed using analyses of past experiments and established theoretical relations involving step nucleation, step propagation, macrostep formation, and competition among crystal surface regions for the available vapor. For growth in constant environmental conditions, the model shows that branches should have nearly uniform width and no sidebranches due to a process involving periodic formation of macrosteps on the leading prism faces. The period should be shorter, and thus the branches narrower, when the growth rate is faster. When there is a sudden change to a faster-growth environment, these macrosteps should form closer to the tip and the step nucleation rate should increase, a situation that allows an additional set of macrosteps to originate from each side vertex, causing sidebranches to sprout. The above predictions are shown to agree with a range of observations. When the macrostep model is extended to the fastest growth regime near -14 °C, it can explain several other previously unexplained phenomena including the cause of the apparent tip rounding, why flat faces appear during sidebranch formation, and why growth at the fastest rate in the atmosphere often produces fernlike dendrites with high sidebranch density. Finally, the symmetry in the Nakaya habit diagram at approximately -14 °C is shown to follow from the peak in the prism-face growth rate near this temperature.

Introduction

Because of their intricate patterns and widespread occurrence, snow crystals have long motivated scientific study. Snow crystals also play an important role in meteorology, particularly in the formation of precipitation but also in other atmospheric processes as well. Even so, many of their general features have not been satisfactorily explained at the level of crystal growth surface processes. The purpose here is to describe how the generation and motion of steps on crystal surfaces can explain common features on branched snow crystals, such as features *a–j* on the dendrite in Figure 1 and features on simpler branched snow crystals such as those in Figure 2. This approach is also used to explain the experimental finding¹ that the branch width is narrowest when the crystal grows at a temperature near -14 °C in a water-drop cloud and also the finding that sidebranches can form by increasing the growth rate through either a humidity or temperature change.^{2–4} Considering the many numerical calculations of dendrite growth (e.g., refs 5–12), the semiquantitative, three-dimensional (3-D) approach here may at first seem unlikely to shed light on the topic. However, unique features of snow crystals are shown here to be important for their growth, whereas even the most detailed numerical models have not treated the unique 3-D growth features of snow crystals. For example, the 2-D numerical modeling of snow crystals by Yokoyama and Kuroda⁵ could reveal the detailed process of branch formation, but the branches only weakly resembled those of real snow crystals. The reason for the weak resemblance in that study and other numerical modeling studies is probably related to the lack of two important processes: step (i.e., layer) nucleation on prism faces and



Figure 1. Dendritic snow crystal. Specific features *a–j* are discussed in the text. The crystal was collected as it fell to the ground, and its size is about 1–2 mm across. Image is from ref 69, courtesy of Tsuneya Takahashi of the Hokkaido University of Education.

the large vapor sink on the branch backsides, both of which have key roles in the theory described here. Hence, the relatively simple 3-D approach in this paper may be useful not only for giving relatively simple

* To whom correspondence should be addressed. E-mail: nelson@sci-cubed.org.

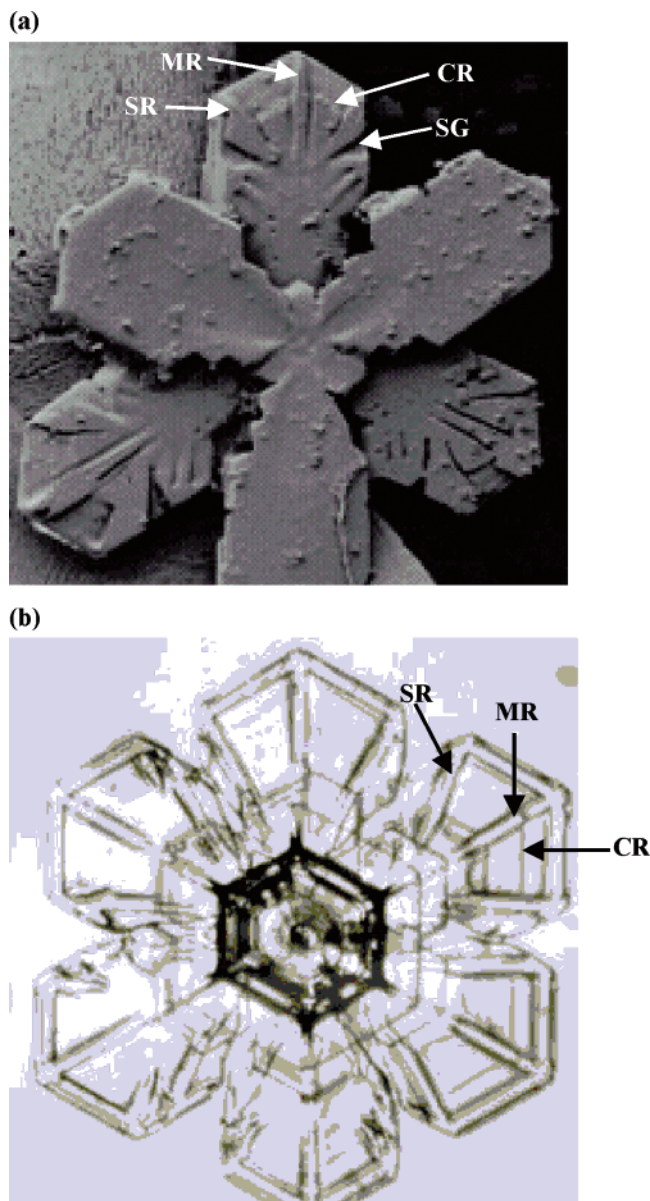


Figure 2. Broad branch (a) and sector plate crystal (b) that were collected at the ground. The main rib MR, side rib SR, side groove SG, and cross rib CR are labeled. SEM image in (a) shows both front and backsides of the branches. Both levels are clearly distinguished. This image is from ref 65, courtesy of Eric Erbe of the USDA. The ribs appear wider and more flat-topped than those on other crystals, which might be due to a slight bit of growth in near-equilibrium conditions after the crystal fell below the cloud. The crystal in (b) is shown in transmitted light (from ref 69, courtesy of Tsuneya Takahashi). Crystal sizes are probably less than 0.5 mm across.

explanations of inherently complex crystallization features but also for identifying the relevant processes that should be included in more detailed numerical studies.

Of the various growth mechanisms, step nucleation has long been known to be important for snow crystal growth. In 1972, Knight argued¹³ that the drastic snow crystal habit changes, which occur over 1–2 °C temperature changes in the Nakaya habit diagram, indicate that the primary growth mechanism is step nucleation. Then, in 1976, Yamashita proposed¹⁴ a growth law based on step nucleation that explains the directions of the branches and sidebranches. Later, Frank showed that prism faces, growing by step nucleation, would

develop pit-like features (which he called lacuna) that lead to the formation of six sets of branches in which one in each set becomes stunted.¹⁵ But despite these and many other studies, neither the branch structure nor the sidebranching mechanism has been adequately described. Moreover, step nucleation is not the only important growth process; this paper also describes the importance of macrostep formation and the growth of noncrystallographic regions on branch backsides. Taken together, these processes can explain branch growth and sidebranching in snow crystals.

Definitions

The basic ice crystal shape is a hexagonal prism with basal faces {0001} on top and bottom and six prism faces {1010} around the sides (Figure 3a). Here, basal and prism faces mean macroscopically flat, stepped surfaces (vicinals) with orientations that are practically indistinguishable from basal or prism orientations. When the surrounding temperature is between about –12 and –18 °C and the supersaturation exceeds several percent, this basic shape can only exist when the crystal is small; when the crystal exceeds a certain size, it grows into a six-branched crystal, as sketched in the sequence of Figure 3b–f. Each branch points in an α -axis direction between adjacent prism faces. Most branches are idealized here as being bound by a top basal face, two leading prism faces on either side of the leading vertex (i.e., outermost tip), two parallel side prism faces, and a tapered, largely noncrystallographic backside that is thinner near the tip than it is near the center of the crystal. Visible ribs often run along some of the growth directions, whereas some lines are parallel to the prism faces.¹⁶ These and other features are marked on the crystals in Figure 2. On dendritic crystals, sidebranches sprout from the side vertex of a branch and then grow along an α -axis. The growth rate R and growth direction of each face are defined to be normal to the surface (Figure 4a). Finally, the names of the crystal forms are from Magono and Lee¹⁷ (ML): “sector plates” are crystals with wide sectorlike (i.e., pie-slice shape) branches (Plb in ML); “broad branch crystals” also have wide branches, but the side faces are roughly parallel and longer (Plc); “stellar crystals” have long, narrow branches (Pld); “dendrites” are crystals with sidebranches (Ple); and “fernlike dendrites” have a high density of sidebranches (Plf). Some variations to these forms are discussed later.

Background Theory and Assumptions

Snow crystals grow while falling through an environment containing water vapor, air, and supercooled water drops. As such, growth may be influenced by vapor diffusion, heat conduction, ventilation, impurities, and collisions or near collisions from water drops.¹⁸ In addition, their growth is greatly affected by surface processes.^{19–22} However, as the goal here is to determine the mechanisms of branch growth and sidebranch formation, we include only vapor diffusion and surface processes because these processes have the largest influence on growth. The surface processes are likely influenced by the surface disorder that has been partly revealed experimentally;²³ nevertheless, studies^{20–22}

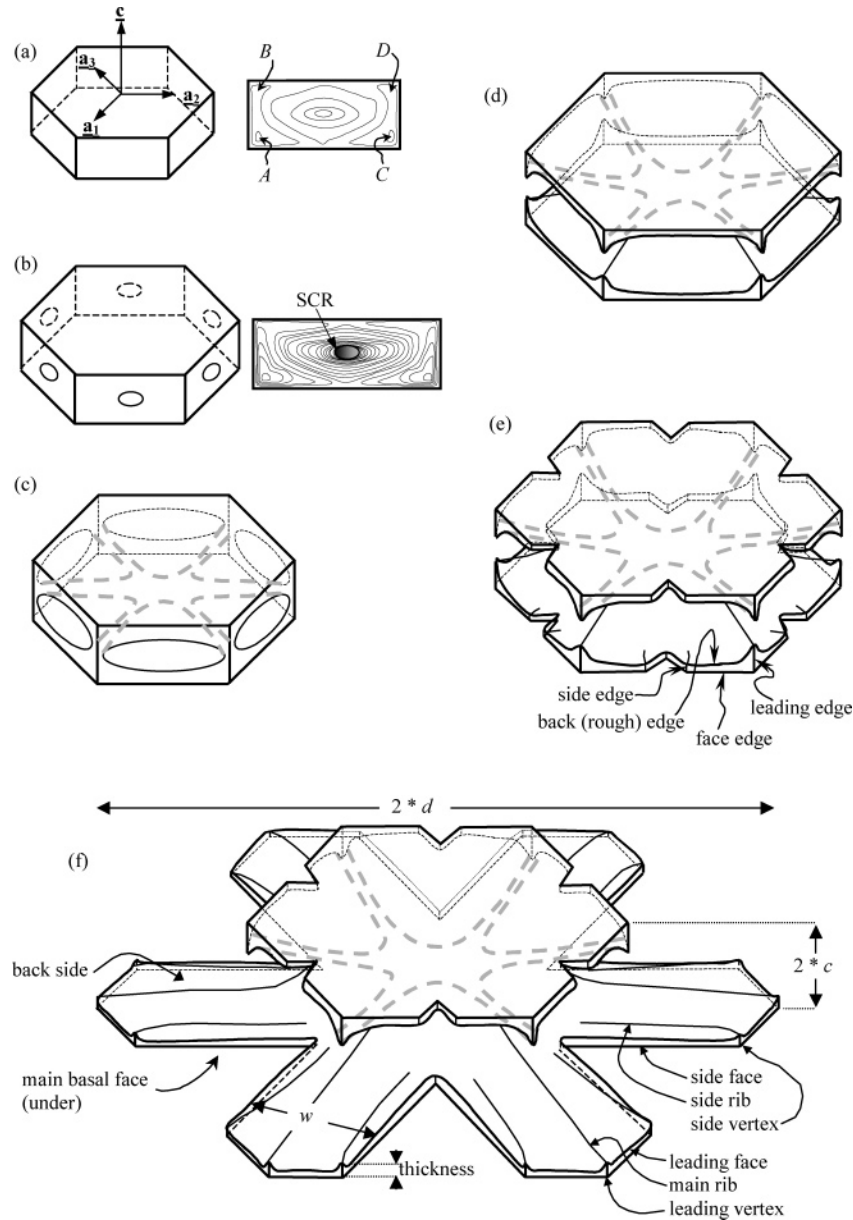


Figure 3. Development of ice crystal (a) into a six-branched snow crystal (f). In (a), steps nucleate at A and C (front view of prism face at right), then spread fastest along the edges before closing in on the center. Crystal in (b) has a step-clumping region (SCR) in each prism face center, which expands as the crystal grows (c) to (e). [To fit on the page, crystal sizes are scaled back as growth proceeds in (a) to (f).] In (d), the SCR cuts the prism–prism edges to form the two-level structure, which develops further to divide each level into six main branches (e). In (f), the branches on the bottom level grow in the direction of the basis vectors \mathbf{a}_i . Sketches are based on observations and similar sketches in refs 14 and 15. The branch width w is often nonuniform, and the branch thickness varies from point to point as discussed in the text. In this example, the bottom had a slightly greater vapor supersaturation than the top, so steps did not nucleate at B and D in (a) and the bottom-level branches grew faster than the top-level branches.

show that the surface steps on ice follow the general predictions from the relatively simple surface diffusion theory in Burton, Cabrera, and Frank, hereafter BCF.²⁴ As a result, we assume that surface diffusion of ad-molecules to steps occurs but do not make any specific assumptions about surface structure or the migrating species. Finally, although several researchers have suggested that migration of ad-molecules from one face to another can significantly influence the growth shapes,^{15,25–27} this process will be neglected because it appears to have little influence on growth for the conditions considered here.²⁸

Each point on a crystal face advances normal to itself at rate $R(i)$, where the face is labeled with index i . BCF

showed that this rate is generally less than that given by the “linear law” in which the growth rate at point x on the face is proportional to the local vapor supersaturation at the surface $\sigma_s(i, x)$. (In reference to the vapor, “at the surface” means at a distance of the vapor mean-free path from the surface.) The linear law holds for surfaces with a high density of steps in which the ad-molecule desorption rate has the equilibrium value.²⁹ This occurs when the step spacing y is significantly less than the ad-molecule migration distance x_s and the surface generally appears curved. In the BCF surface diffusion model, the fractional reduction in growth rate from the linear law (R/R_1 in BCF), now called the condensation coefficient α , is inversely related to y/x_s

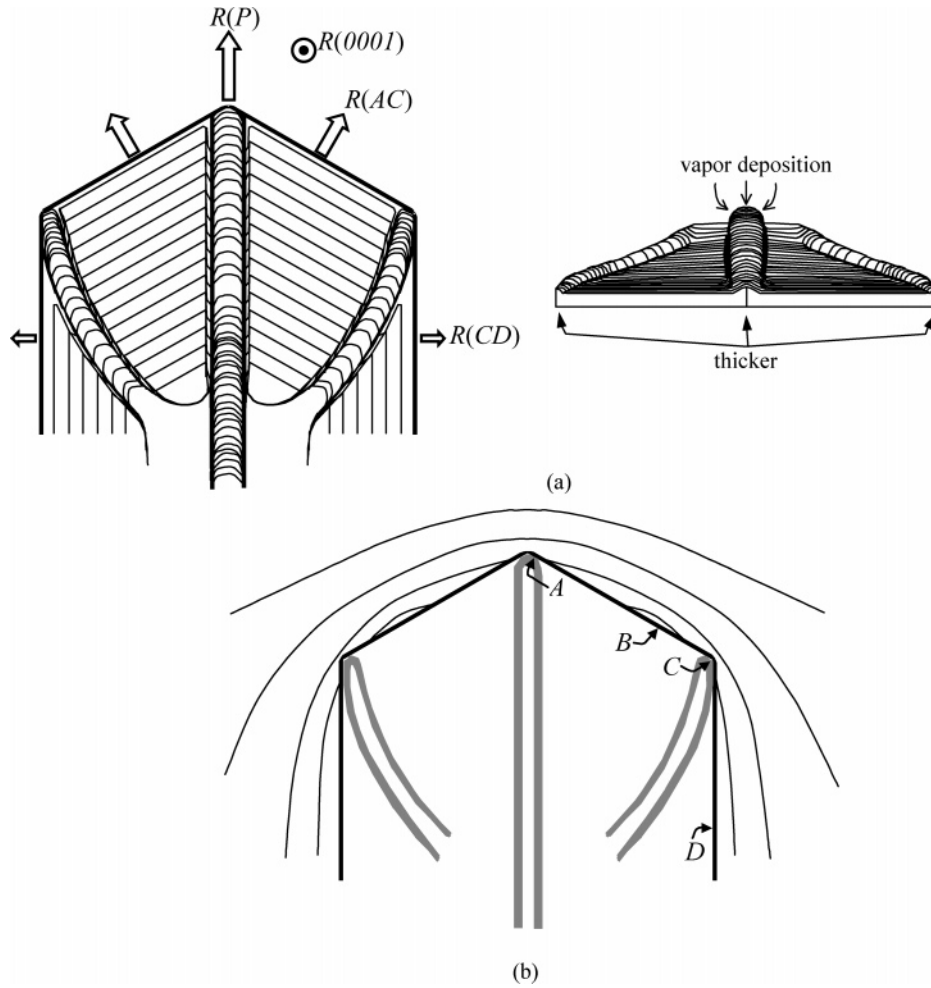


Figure 4. Structure of the backside and implications for the vapor density contours around the branch tip. The plan view in (a) (left) shows the main rib (MR) in the center and the side ribs (SR) on either side. (Cross ribs are not shown.) The thin lines are approximate contours to show surface relief—not surface steps. Narrow channels exist on both sides of each rib. The side view on the right shows how the ribs protrude above the surface and grow. In this sketch, the lines are hypothetical vertical slices to show the relief—also not surface steps. The notation for the normal growth rates R are also shown. Transmitted-light view (b) shows the resulting MR and SR that are typically seen (e.g., Figures 1, 2b, 6, and 8). The implication of the main and side ribs is the σ_s -maxima at points A and C (and thus a σ_s -minima at B), as shown by the vapor density contours.

(e.g., $\alpha = (2x_s/y) \tanh[y/2x_s]$ for symmetric step capture). However, the steps must first be created on a face, and at this special point (or points), the step-source point, the value of y/x_s , and hence α depends on both the local supersaturation at the step source $\sigma_{ss}(i)$ and the step-formation mechanism. The flatness of most basal and prism surface orientations suggests that their step densities are not high enough for the linear law, and thus $R(i)$ should depend nonlinearly on $\sigma_{ss}(i)$. But, unlike the pure-vapor case in BCF, the vapor supersaturation varies along snow crystal surfaces and has a maximum $\sigma_{ss}(i)$ at the step source on a corner of each face. Also, the values of $\sigma_{ss}(i)$ are less than the supersaturation far from the crystal σ_A because each growing surface region locally depletes the surrounding air of vapor molecules. (Because of vapor supersaturation gradients in the air around the crystal, the nonlinear relation between R and σ_{ss} is difficult to test directly; nevertheless, experiments on ice in a pure vapor environment^{30–32} and modeling of snow crystal growth^{5,28,33,38} support this nonlinear assumption.) In short, snow crystal growth involves a nonlinear response of each face to the local conditions, superaturation gradients along, and normal

to, each face, and competition for vapor among the various surface regions.

Although this paper mainly uses general arguments involving the above quantities, it is useful to refer to their theoretical relationships. Thus, the equations and definitions that will be referred to throughout the paper were put together for easy reference below.

$$R(i) = k_1 \alpha(i, x) \sigma_s(i, x) = k_1 \alpha_s(\sigma_{ss}(i)) \sigma_{ss}(i) \quad (1)$$

$$\alpha_s(\sigma_{ss}(i)) \leq \sigma_s(i, x') / \sigma_{ss}(i) \quad (2)$$

$$\sigma(r) = \sigma_A - k_2 \sum_i R(i) A_r(i) h_i(r) \quad (3)$$

with

- $\alpha(i, x)$: reduction of growth rate at x on face i from the linear law; ranges from 0 to 1
- $\sigma_s(i, x)$: vapor supersaturation (fractional deviation from equilibrium) at point x on face i (σ in BCF)
- $\alpha_s(\sigma_{ss}(i))$: α value at the step source on face i ; is highly nonlinear in σ_{ss} when i is a prism face
- $\sigma_{ss}(i)$: vapor supersaturation at the step source on face i ; is the maximum $\sigma_s(i, x)$ on the face

σ_A : ambient (far-field) vapor supersaturation; is $\sim 0.13\text{--}0.18$ for most conditions considered here
 $\sigma(\underline{r})$: vapor supersaturation at any point \underline{r} outside of the crystal; equals σ_s at the surface
 $A_r(i)$: area of face i
 $h_i(r)$: solution of diffusion equation for unit flux to face i ; decreases with distance from the center of face i
 x_s : mean displacement of ad-molecules on prism face; is expected to be $\sim 0.1\text{--}1\ \mu\text{m}$ for ice^{25,31}
 $y(x)$: step spacing at x ; is largest at the step source
 SCR: step-clumping region; revealed as a macrostep or pit in a face
 σ_s/y relation: on a face, $y(x)$ is relatively small at x where $\sigma_s(i,x)$ is relatively small

In the left equality of eq 1, the values of α and σ_s individually depend on position x on the face, but their product does not. (The value of k_1 is given in the appendix.) In particular, the equality holds at the step-source position on the face, which is the second equality in eq 1. The reason that the growth rate is uniform, that is, the same everywhere on the face, is because the steps slow down in low- σ_s regions and, as a result, get closer together. Where the steps are closer, the surface captures more ad-molecules and thus α is larger.^{5,15,37,38} This important relation between σ_s and y is hereafter called the “ σ_s/y relation”. Equation 2 follows from the second equality of eq 1 and the limitation that α cannot exceed unity. This equation is useful because it means that the face remains intact [i.e., has uniform $R(i)$] between the step source and the edge of the face at x' . Finally, we will refer to eq 3 to estimate whether the growth on some face j significantly affects growth on some other face k . This is done by evaluating the relative magnitude of term j at the point of the step-source position on face k . At distances exceeding the size of face j , the function $h_j(r)$ decreases roughly in inverse proportion to the distance from face j to point r . (k_2 is positive,^{28,33,34} but its value is not needed here.) To make the system of equations complete, one must describe how the condensation coefficient of each face depends on the local supersaturation [i.e., $\alpha_s(\sigma_{ss}(i))$]. These important relations are described next. In the rest of the paper, the face index i will be dropped when either the face under discussion is obvious or the discussion applies to all faces.

The functional dependence $\alpha_s(\sigma_{ss})$ is largely determined by the step-formation mechanism. For snow crystals, these mechanisms are still being debated,³⁹ and new mechanisms have recently been proposed.^{40,41} Nevertheless, for the temperature range in which branched crystals grow, a general understanding of the step-formation mechanisms for the basal and prism faces has emerged. The basal faces likely grow by the spiral step mechanism in which $\alpha_s \sim \sigma_{ss}^n$ with $n = 0, 1$, or 2 (refs 41, 24, and 42, respectively). The important feature of this mechanism is that growth occurs at all supersaturations, but it is slower than the step-nucleation mechanism at high supersaturations.^{43,44} For the prism faces, experiments,^{25,31,45} modeling,^{28,38} and general observations^{15,46–48} indicate that both spiral step sources and step nucleation can supply steps to each prism face when the crystal is small or the supersaturation is below a few percent. At larger sizes and higher supersaturations, which is the case of interest here, step

nucleation is thought to provide the main source of steps.^{28,35,36,48} Although steps being nucleated on growing snow crystals have not been observed directly and spiral steps might have a non-negligible influence on growth in some cases, step nucleation will be the assumed growth mechanism for the prism faces on the branches because previous studies have shown that the mechanism is useful for explaining many observed features of snow crystals.

The key feature of step nucleation is its extreme nonlinearity. For snow crystals, the rate is predicted to increase roughly as $\exp[-48\sigma_{cr}/\sigma_{ss}]$ when σ_{ss} is near the critical supersaturation σ_{cr} (refs 28 and 48). On the prism face, σ_{cr} is about 0.004 for the temperatures considered here, although it may increase below $-15\ ^\circ\text{C}$ (ref 70). One consequence of the rapid rise in nucleation rate is that, in the quasi-periodic regime of $\sigma_{ss} > \sigma_{cr}$, steps repeatedly nucleate at the highest supersaturation point or points on the surface.⁴⁹ The nucleation process actually responds to the ad-molecule supersaturation (labeled σ_s in BCF), a quantity that is depleted to the equilibrium value (i.e., 0) at the steps and approaches the local value of σ_s at distances exceeding x_s from the step. This is the reason that the steps are nucleated quasi-periodically at the highest- σ_s points; moreover, due to both the lower σ_s and closer steps away from the highest- σ_s points, steps should rarely nucleate anywhere else. Furthermore, because the nucleation rate rises so rapidly with σ_s , steps generated at the highest- σ_s points will eventually overtake those that are nucleated anywhere else. Except in the initial growth period of the prism faces, in which all four corners of a face can be equivalent, the prism faces likely have just one point on the face with the highest surface supersaturation. For these reasons, we assume that each prism face on a branch has only one step source. This is an important assumption.

Branch Formation

The use of these equations and the various assumptions are illustrated by applying them to the initial stages of snow crystal growth. In Figure 3a, the maximum supersaturation is at corners of the prism face,³⁸ so nucleation occurs at corners $A\text{--}D$ ^{15,50,51} (or some subset of these points if vapor asymmetries exist). In the sketch, the new steps spread fastest along the edges where σ_s is relatively high, and then they slow down and converge on the face center where σ_s is lower. When the crystal grows in Figure 3b, the face areas A_r increase, thus increasing the difference in σ_s across the face. From the σ_s/y relation, the steps become closer in the center. At some size, eq 2 is violated, that is, $\alpha_s > \sigma_s/\sigma_{ss}$, and the steps clump together in the center, forming a pit.^{5,15,33,38,46} (Some authors call this a “facet instability”, “morphological instability”, or “facet bending”.) The edge of the pit has a steep wall of clumped-up steps, hereafter a step-clumping region (SCR) or macrostep. As the face grows, the SCR boundary usually expands outward,⁵³ as in Figure 3c, and eventually reaches the prism–prism edge, thus cutting the crystal into two levels in Figure 3d. This sketch shows the familiar star-shaped pattern in the interior of many snow crystals. With further increase in size, the SCR

reaches the basal-prism edge in the middle, causing one or both levels to sprout six branches (Figure 3e). The example here also shows that fast-growing faces have at least one edge that is defined by an SCR; thus, an increase in crystal size or a change in conditions may cause the SCR to quickly adjust its position. Another important feature is the slight thickening of the prism face near the leading edge because this will later be shown to generate the main rib.

When both levels sprout six branches, slight asymmetries in the environment will cause the branch on the top or bottom level to grow further than the other, thus causing the shorter branch to remain stunted.¹⁵ In general, the stunted branches can be on either level;¹⁶ in Figure 2a, three are on top and three are on bottom, and in Figure 2b all six appear to be on one level. As the branch grows, the slightly thicker prism face region at the tip leaves a “track” in its wake, hereafter called the main rib. This rib shows that the branches grew along an a -axis. Strict adherence to these growth directions occur due to the equal rate of step nucleation at the leading vertex on both prism faces.^{14,48}

Branch Growth

Initial Branch Size. The initial width of a branch is largely determined by the ice crystal size when the branches first sprout. This size can be estimated from eq 2 as follows. Violation of eq 2 ($\alpha_s > \sigma_s/\sigma_{ss}$) indicates the break-up of a face by the formation of an SCR and thus is the first stage of branch formation. Other things being equal, this should occur at a smaller face size when α_s is larger because σ_s can decrease only very slightly from the vertex value σ_{ss} before $\alpha(i,x)$ saturates at unity and the steps clump into an SCR. For a fixed gradient in σ_s across a face, a small decrease in σ_s between the vertex and the SCR implies a small face. Hence, fast-growing faces, which have relatively large α_s , should be relatively small. It follows that crystals originating in environmental conditions that produce fast growth go through a sequence like Figure 3a–f at a smaller size and thus have narrower branches initially. In agreement with this prediction, Yamashita’s experiments on snow crystal growth in a water droplet cloud¹⁴ showed that the maximum crystal dimension at the stage of Figure 3b is about 50–100 μm at -13°C and about 10–30 μm in the faster-growing temperature regime of -14 to -16°C .

Interior Markings. The main rib “MR” and side ribs “SR” in Figure 2 are common interior markings on the backside of snow crystal branches. Point a in Figure 1 also shows side ribs that terminate at the side vertex, and point e shows a side rib that becomes the main rib of a sidebranch. Frank discussed the initial formation of the main rib and the growth of the main rib normal to the backside,^{15,46} but a mechanism by which ribs propagate with the vertices and form on new vertices has not been given. A plausible mechanism is as follows. The face region near a prism–prism edge on a leading face should be thicker if it has a local maximum in σ_s because steps must travel further along the edge before clumping (as sketched in Figure 5c). In fact, any convex vertex should have a local maximum in σ_s because it slightly sticks out into the vapor. This means that the backside near the leading faces should be slightly

thicker right behind all convex vertices, including the leading edge and side edges. These thicker regions should remain, and even grow, after the face advances, thus leaving behind a rib as a “track” of the thick face region on the advancing face. Therefore, even if the rib on the backside is initially only a slight protrusion, as in the right side of Figure 4a, it can become thicker and slightly wider as it grows due to locally high vapor deposition to protruding areas. Also, due to the local vapor sink on the rib, trenches develop in the vapor-depleted region on both sides of the rib, which tend to highlight the ribs.¹⁵ But, despite the effective roughness of these features, their growth is not rapid because they are within a relatively large area of growing surface.

Despite the local supersaturation maximum at the side vertex, the main vertex has the highest σ_s on the leading faces. This “overall” maximum is regarded as a simple consequence of the main vertex being the furthest from the crystal center. (Support for this claim is the observation that the leading prism faces on both sides of the main vertex grow at the same rate.^{14,48}) Therefore, referring to Figure 4b, there is a local minimum on the leading faces such that $\sigma_s(A) > \sigma_s(C) > \sigma_s(B)$ and the resulting vapor density should look like that in the drawing. This minimum will play a major role in the branch features described in later sections.

In addition to the ribs, “cross ribs”, or lines parallel to the leading face occur, as marked CR in Figure 2. According to the crystal dissections by Nakaya and Yamazaki,¹⁶ some of these lines protrude from the backside, much like the main and side ribs. The cross ribs might initially arise by a slight thickening or thinning of the leading faces during fluctuations in the cloud conditions, a mechanism that can explain their positions being about the same on all branches. As argued later, the branch width should also respond to changes in cloud conditions, so the cross ribs may be linked to changes in branch width in some cases. Some evidence for the latter is the line at point h in Figure 1. Still, the source of the cross ribs remains unclear.

Uptake of Vapor on the Backside. Branch section profiles¹⁶ and photomicrographs strongly suggest that the backsides are largely composed of noncrystallographic orientations. If so, these relatively large-area, rough regions should grow according to the linear law and thus capture a relatively large amount of water molecules. This implication is supported by measurements of crystal growth rates and total mass uptake¹ as follows. The mass uptake $(dm/dt)_m$ equals the sum of the area of each surface region times the growth rate normal to the region times the mass density of ice. I estimated the mass uptake to the face regions of the crystal by calculating the total mass uptake over the leading faces, side faces, and top basal face of each level, and then compared the sum to the measured total mass uptake. The results in Table 1 show that the face regions account for only 13–23% of the total mass uptake; or equivalently, the backsides and center regions account for 77–87% of the total mass uptake. The growth rates should be slowest near the center regions of the crystal (i.e., inside the original pits in Figure 3b,c), so most of this noncrystallographic mass uptake must come from the branch backsides. Thus, branched snow crystals

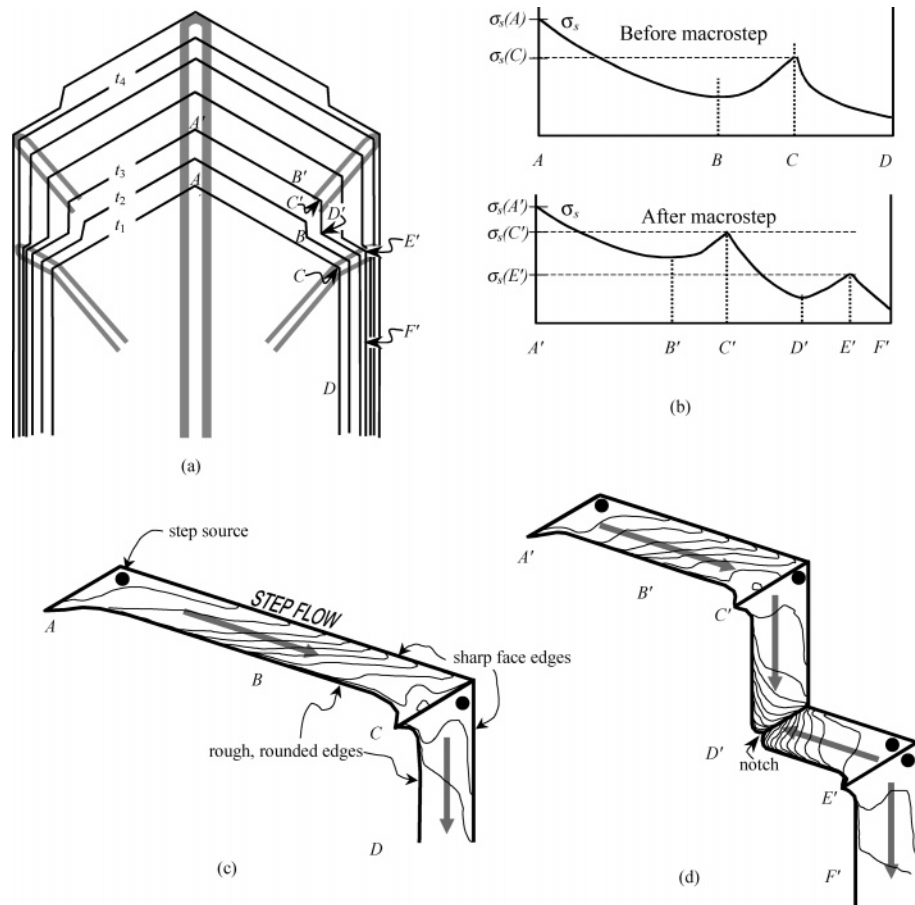


Figure 5. Macrostep model of branch growth for nearly constant growth conditions. (a) Branch perimeters at a succession of times $t_1 < t_2 < t_3 < t_4$. (b) At t_1 , point B is the σ_s -minimum on the leading face, as sketched in the top plot of σ_s . The bottom plot applies to times from t_2 to t_4 . (c) Steps are generated at A , flow toward C , but slow and cluster near B due to the lower supersaturation there, and then spread out as they speed up toward C . Step motion is fastest along the leading, side, and face edges. Solid circles are step-nucleation sites. (d) Macrostep that developed at B at time t_2 , produced a new side vertex C' while reversing the step flow between D' and E' . The inside corner $C'D'E'$ effectively vanishes at t_4 . Then, the cycle repeats, with each new macrostep generating new side ribs that are shown as thick gray lines in (a).

have the curious property that their external dimensions are controlled by the growth of flat faces whereas their total mass is dominated by growth to the rough regions. Moreover, as these major mass sinks are adjacent to the leading and side faces, the growth rates on these faces must be significantly reduced by the presence of the backsides, particularly when the branches are wide.

Macrostep Branch Growth Mechanism. Observations of branch widths present a puzzle. According to the step-nucleation mechanism, the growth rate of the side face $R(CD)$ (Figure 4) is governed by $\sigma_s(C)$, which, judging from its distance from the crystal center, is probably nearly equal to $\sigma_s(A)$. Thus, if a main branch grows with complete leading and side faces, the leading faces should continue to widen at rate $R(CD)$ during growth, eventually becoming very wide. Indeed, wide branches are common on sector plates, which grow slower than the other branched crystals. However, by such reasoning, the longest branches should be the widest. Instead, the opposite occurs: observations show that the longest branches are the narrowest. For example, at an ambient temperature of -14.4 °C, the branch length is nearly 580 μm after 10-min of growth, the longest of all crystals and more than twice that of the crystal at -16.8 °C. Yet the branch width at -14.4

°C is at most 80 μm , less than half that at -16.8 °C and less than that at all other temperatures (Table 2).

The only previous attempt to explain narrow branch growth appears to be that of Mason et al.²⁵ They suggested that growth steps from the tip spread outward and bunch together due to some random perturbation at a distance of $\sim 10x_s$ from the tip. A rapid succession of such bunched steps, each new one starting before the last one is "complete" was argued to produce narrow branches. In contrast to their explanation, random perturbations are not needed for the mechanism described here because SCRs must form where α rises to unity. Moreover, the mechanism proposed here can also be used to examine the rib structure and side-branching.

A solution to the branch width puzzle follows from the processes sketched in Figure 5. Growth of the leading face is generated by step nucleation at the rate controlled by σ_s at A , the step source [i.e., $\sigma_{ss}(AC)$]. At time t_1 , steps at A flow toward C , but, in doing so, they pass through the σ_s -minimum at B (Figure 5b, top), which, by the σ_s/y relation, has the smallest step spacing on the face (Figure 5c). As the side face grows, the leading face widens and, just like the face in Figure 3a,b, steps eventually clump at B . But instead of a pit forming, the SCR becomes a macrostep because the

Table 1. Face Growth Rates and Mass Uptakes^a of Snow Crystals with Insignificant Sidebranch Development after 10 min of Growth in a Cloud Containing 0.1 g m⁻³ of Supercooled Liquid Water^b

T [°C]	$R(P)$	$R(AC)$	$R(CD)$	$R(0001)$	$(dm/dt)_m^c$ ($\times 10^{-12}$)	$(dm/dt)_f$ ($\times 10^{-12}$)	f_r
-13.3	0.50	0.43	0.10	0.0074	13.7	3.10	0.77 ^c
-14.0	0.59	0.51	0.085	0.0067	19.4	3.23	0.83
-14.4	0.97	0.84	0.067	0.0063	21.3	2.91	0.86
-16.0	0.53	0.46	0.10	0.0068	13.3	1.70	0.87
-16.8	0.47	0.41	0.16	0.0066	7.08	1.14	0.84

^a Based on data in ref 1. The crystal growth speeds $R(P)$ and $R(0001)$ are in $\mu\text{m s}^{-1}$, and mass uptakes $(dm/dt)_m$ in kg s^{-1} are interpolations from their own measurements as listed in their Table 2. Growth speeds $R(AC)$ are deduced from $R(P)$; $R(CD)$ equals $w/2$ from the images divided by the growth time. The mass uptakes of all faces $(dm/dt)_f$ are estimated from the face growth rates and estimated face areas. The “rough fraction” f_r is the fraction of mass uptake not occurring on faces $[(dm/dt)_m - (dm/dt)_f]/(dm/dt)_m$. The largest uncertainties are the thicknesses of the prism faces, which have not been measured. This calculation assumed that the thickness decreased linearly with distance from the crystal center, ranging from c at the crystal center to zero at the primary vertex. Effectively, this meant that that leading prism faces were less than $1 \mu\text{m}$ at -14.4°C and more than $1 \mu\text{m}$ at -16.8°C . ^bFace labels P , AC , CD , and 0001 are defined in Figure 4a. ^cMass m was determined by melting the crystal and measuring the diameter of the liquid drop. ^dThis is a slight underestimate due to an overestimate of the face area on the branches.

Table 2. Branch and Crystal Dimensions^a for Snow Crystals with Insignificant Sidebranch Development after 10 min of Growth in a Cloud Containing 0.1 g m⁻³ of Supercooled Liquid Water

T [°C]	σ_A	d	w_{\max}	w	d/w_{\max}	c	type
-13.3	0.139	303	156	121	1.9	9.5	broad branch
-14.0	0.147	357	137	102	2.6	8.1	broad branch ^b
-14.4	0.151	580	80	<80	7.2	7.3	stellar ^c
-16.0	0.169	316	170	125	1.9	8.4	broad branch
-16.8	0.179	281	195	195	1.4	9.6	sector plate

^a On the basis of data in ref 1. Except for the maximum branch width w_{\max} , the values are averages of all six branches from photographs g–k in Figure 1 of ref 1. Units are in μm . The crystal thicknesses $2c$ are interpolations from data in their Table 2. ^b Shown in Figure 6a. ^c Shown in Figure 6b.

steps flow from A only. (The macrostep fronts are usually sketched here and elsewhere as flat, although they may initially be curved.) At times t_2 and t_3 , the macrostep develops into a new side face $C'D'$ with an inside corner at D' , so there is also a new, narrower leading face $A'C'$ and a small section of the former leading face $D'E'$. However, the step flow on face region $D'E'$ has changed because the macrostep-generated face $C'D'$ is a barrier that prevents steps from A' from reaching E' . Therefore, the steps on $D'E'$ should come from the vertex at E' , a reversal of the previous situation (Figure 5d). This change should change the side rib direction from being less than 60° to the main rib to being nearly 60° . (As with the main vertex, the growth direction of a vertex such as E' is along an a -axis when the step source is very nearly the same point for adjacent prism faces.) Points “SR” in Figure 6a show this change of direction of the side ribs. Initially, C' is near a σ_s -minimum on $A'C'$. But after growing a bit, it should become a local maximum like the original C . Hence, the step flow between A' and C' becomes just like that of the former A and C , the step flow between C' and D' becomes just like that of C and D , and a new side rib develops (Figure 5d). The new supersaturation profile is in Figure 5b, bottom. The side face $E'F'$ grows

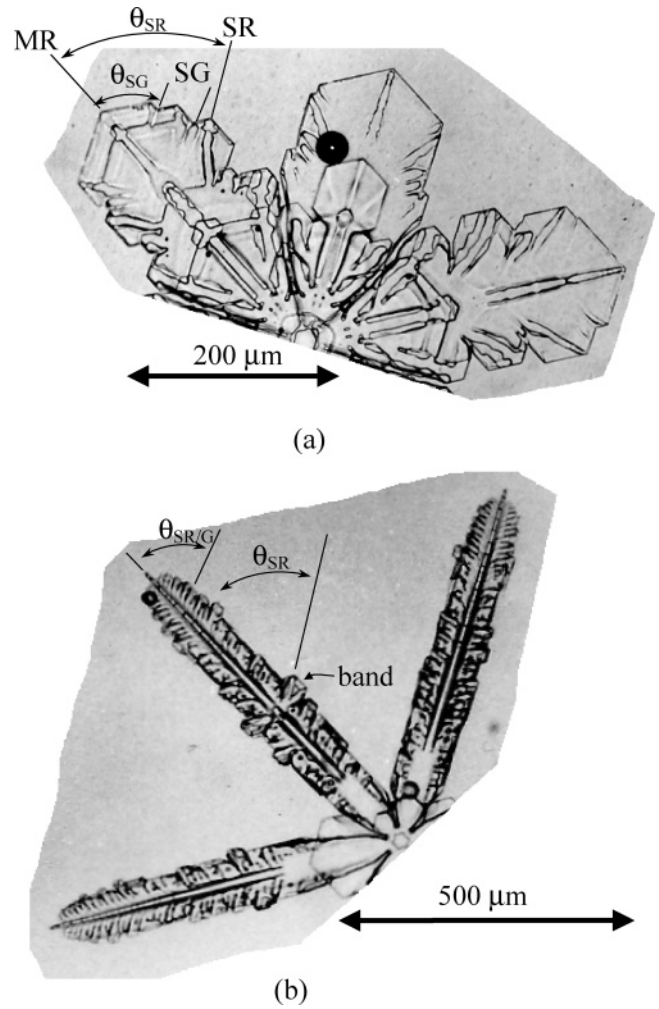


Figure 6. Broad branch and stellar crystals grown in a vertical supercooled cloud wind tunnel for 10 min. The liquid water content was 0.1 g m^{-3} , and conditions were nearly constant. The images are from Figures 1h and 1i in ref 1 but are reproduced and enlarged from the original photographs supplied by T. Takahashi. The broad branch crystal in (a) grew at -14.0°C . Lines are drawn parallel to the main rib MR, two side grooves SG, and a side rib SR. The angle θ_{SG} is 62° for one SG and 64° for the other. The angle θ_{SR} is 56° . The black circle is probably a water droplet that froze to the surface. The much-faster-growing stellar crystal in (b) grew at -14.4°C . In the dense side-rib/side-groove region, the angle $\theta_{SR/G}$ is 69° , whereas the side rib on the band has $\theta_{SR} = 57^\circ$. The sharp points at the tips of (b) arose from accidental evaporation of the face side of the branch tips before obtaining the image. (The rib on the backside was apparently submerged in oil during a brief period of evaporation.) The growth rates and dimensions of these crystals are in Tables 1 and 2.

by step nucleation according to the σ_s value at E' ; however, the new leading face has surged ahead, leaving E' in a region of lower supersaturation. As α_s is super-sensitive to σ_{ss} , the growth rate of $E'F'$ slows considerably; that is, the side face hardly advances. Meanwhile, at times up to t_4 , the new region of side face $C'D'$ grows at the rate determined by σ_s at C' and thus fills out the inside corner $C'D'E'$. Now the situation is the same as that in the beginning, so the process repeats. The result is that the sides of the branch grow much more slowly than the leading faces, resulting in branches that can be much longer than wide. Thus, even though faces advance by single steps, the growth features are largely

due to macrosteps. For this reason, the model is called the macrostep model.

Another prediction from the macrostep model is that a notch should form at D' (Figure 5d). For the same reason that the prism faces are slightly thicker at convex corners (e.g., points A , C , A' , C' , E'), the minimum in supersaturation at D' should produce a locally thinner face. Indeed, this supersaturation may be particularly low and drop rapidly at D' because $C'D'E'$ forms an inside corner in which D' is depleted of vapor from the two adjacent faces. Thus, a pronounced “notch” may form at D' . As faces $C'D'$ and $D'E'$ advance, this notch should leave a trailing groove in its wake, just as the convex vertices leave a rib. Apparent examples of such “side grooves” are marked “SG” in Figures 2a and 6a. Figure 1 also seems to have a side groove near g . These side grooves should differ from side ribs in two ways: one, the angle between them and the main rib should be greater than 60° because the new side-face $C'D'$ will grow faster than $D'E'$, and the side grooves should be longer than the side ribs because D' is at a σ_s -minimum from the very start of the macrostep formation.

Each time a macrostep forms, the resulting new vertex C' produces another side rib and the inside corner D' produces another side groove. Thus, the branch should have a sequence of side ribs and side grooves along each branch. Indeed, photomicrographs of long narrow branches show such features. Figure 1 (e.g., c) and Figure 6 show several examples, and Bentley and Humphreys,⁵⁵ hereafter BH, has many other examples including images 129:2:2, 135:4:3, 141:2:2, 142:4:3, 143:1:3, 151:2:3, which are labeled as page number/row number/column number.

Branch Width Versus Growth Rate. Because of the highly nonlinear dependence of step nucleation to supersaturation, fast-growing branches should be significantly narrower than slow-growing branches. The argument is as follows.

The step spacing at the main vertex decreases with an increase of α_s , and thus a relatively fast-growing branch has a relatively large value of α_s and consequently a small step spacing at the tip. By the same argument as that used to explain why narrow initial branches form at high growth rates, the macrostep will form closer to the main vertex at high growth rates. If the macrostep forms closer to the tip, the side vertex C (Figure 5) gets left behind in a lower supersaturation while it has a narrower width and thereafter grows much slower than the tip. Therefore, this macrostep model can explain one of the motivating puzzles: why the narrowest branches occur at the fastest growth rates. In addition, the macrostep model predicts that narrow branches have more closely spaced side ribs than wide branches, a prediction that is well supported by observation, for example, in the images in Figure 6.

Rib and Groove Angles. The relation between rib angle and step-source position was previously analyzed for a frost crystal,⁴⁸ and the relation between the groove and sidebranch positions has been discussed for the case of melt-grown dendrites.⁵⁶ Here, we examine both phenomena on snow crystals.

As we have seen, the angle between a given side rib or a side groove and the main rib reflects the relative

growth rates between the faces on either side of the side rib or groove. Moreover, these relative growth rates, and thus angles, can change when the step source for a face moves to a new position. For the broad-branch crystal in Figure 6a, the side grooves (SG) are slightly more than 60° from the main rib (MR), whereas the side rib (SR) is slightly less than 60° . Moreover, several side ribs bend, a feature that was predicted to occur when the step source moved to the side vertex after a macrostep formed. In the stellar crystal of Figure 6b, the numerous, short side ribs have angles that exceed 60° , which appears to contradict the above discussion. However, in this case, the side ribs and side grooves are so close together that they can strongly influence each other. Thus, the side ribs in these cases may exceed 60° because the side groove angles must exceed 60° . In contrast, the side rib on the “band” feature, which is more widely separated from the side groove, has an angle slightly less than 60° . Hence, the predictions from the macrostep model are also in good qualitative agreement with observations of side ribs and side grooves.

Growth of P1b, P1c, P1d, P2a, and P2b Snow Crystals. It is straightforward to apply the model to various branch forms. The difference in growth mode between stellar (P1d) or broad-branch (P1c) and sector plate (P1b) is shown in Figure 7a,b. The stellar branch in Figure 7a is the result of a numerical calculation described in the appendix. It shows how repeated macrostep formation and growth by step nucleation produces a narrow branch. A broad-branch crystal is similar to a stellar, but successive side ribs have larger spacings and the branch width is wider due to the slower rate of step nucleation. As the nucleation rate is decreased ever lower, a low enough step-nucleation rate will be reached so that no macrosteps form on the leading faces. The resulting form is a sector plate (Figure 7b). Each branch widens as it grows, but the widening rate is limited by the closeness of the adjacent branch. Because of this closeness, the side region E becomes noncrystallographic with only a short region near the side vertex CD remaining as a flat side face. Because no macrosteps form on the leading faces in this case, each branch has a single pair of side ribs. Because of the adjacent branch, the side rib angle from the main rib cannot continuously exceed 30° on large crystals. This is consistent with the range of angles from about 27° to 34° on the sector plate in Figure 2b.

A practically limitless number of branch features can arise when the conditions vary. In Figure 7c, the branch grows like the narrow branch in Figure 7a until time t_1 , then the environment changes to slower-growth conditions, and the macrostep formation temporarily ceases, thus allowing the crystal tip to widen at t_2 . If the environment changes back to the original (slightly faster) growth condition at t_3 , a leading-face macrostep will form, thus creating the side vertex C and inside corner CDE . The widening and narrowing has left a slightly wider “band” in the middle of the branch. The process can be repeated if the crystal passes through more environmental fluctuations, leading to a bumpy branch-side. The band resembles a “proto-sidebranch”, and some researchers have called inside corners such as CDE a sidebranch,²² but it is not a sidebranch because new side faces at 60° to the old side faces never

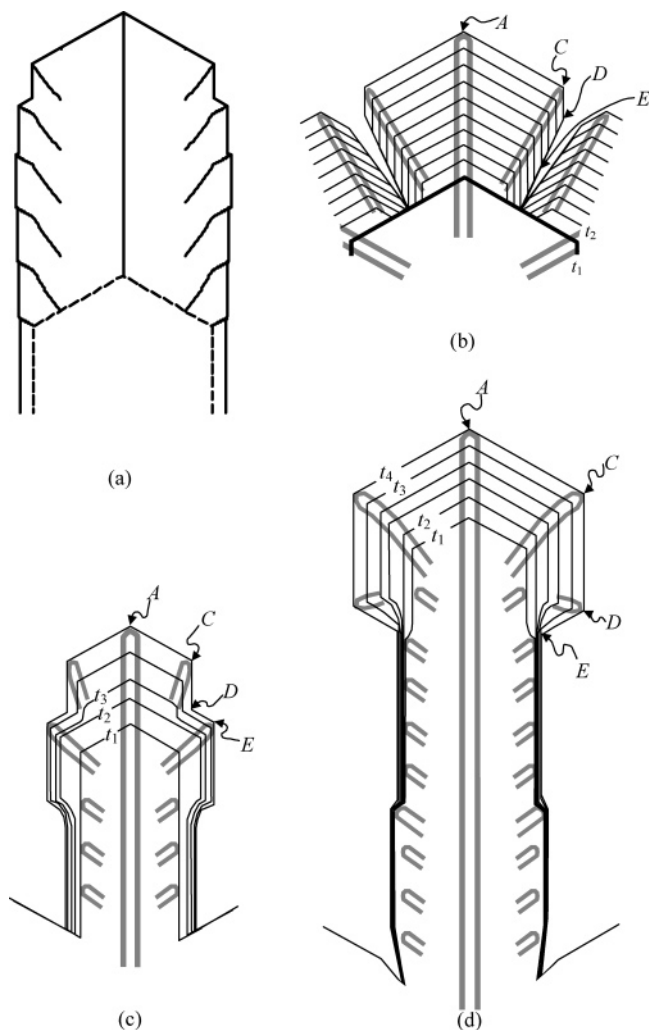


Figure 7. Branch growth under various conditions. (a) Calculation of branch growth under the conditions specified in the appendix. The tip is initially $680.6 \mu\text{m}$ from the crystal center, and the width of the tip is $80 \mu\text{m}$ as outlined by the dashed curve. Side ribs track the positions of the side vertices. The final dimension after 104 s of growth is $801.2\text{-}\mu\text{m}$ long with a width at the base of $92.6 \mu\text{m}$. (b) Successive branch perimeters as a sector plate (P1b) grows. The characteristic features are a lack of leading-face macrosteps and a side-face region *CD* that is short or nonexistent. The region near *E* is generally noncrystallographic. (c) Band feature that arises on a stellar (P1d) or broad-branch (P1c) crystal when growth briefly slows at time t_1 , causing a wider leading face and macrostep on the side face, and then slightly speeds up at t_3 . (d) Macrosteps form on only the side faces when the growth rate decreases, resulting in a hexagonal plate at the end of a stellar branch (type P2a).

developed. Many crystal photomicrographs show branches or sidebranches with one or more such bands (e.g., point *i* in Figure 1, several in Figure 6, and 89:3:2, 141:1:2, 141:2:2 in BH). If the environment for the branch in Figure 7c remained in the slow-growth conditions, the tip would continue to widen as it does at times t_2 to t_3 in Figure 7d. This is similar to the wide tip on the crystal in Figure 1. In Figure 7d, the side faces continue to grow outward, and at t_4 a new prism face *DE* develops at the base. In ML, this growth form is called P2a or “stellar with plate at ends”. A P2a crystal like this can form when the tip region is relatively isolated from the other branches and sidebranches. But when the plates at the end are wide

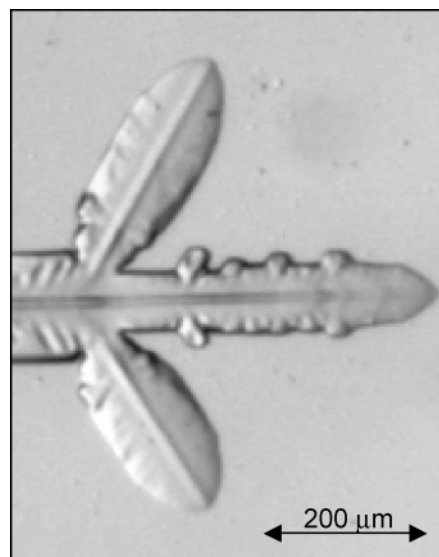


Figure 8. Tip region on a dendrite with a rounded tip. Image courtesy of Charles Knight of NCAR.

enough that they strongly compete with the adjacent branch for vapor or compete with sidebranches near the tip for vapor, face *DE* does not develop, and so this lower side region remains noncrystallographic. Such a region is marked *b* in Figure 1. These growth forms are P2b (“stellar with sectorlike ends”) and P2d (“dendrite with sectorlike ends”), respectively.

In addition to the branch width changes, the branch thickness should also adjust to the conditions. For example, when a plate forms at the tip as in Figure 7d, the tip region should also thicken on the backside, and it may even develop into a second basal face. The latter feature was called a “double sheet” by Nakaya,¹⁶ and even the crystal in Figure 2a seems to show some basal face regions on the backside.

Rounded Branch Tips. Branch tips do not always have clearly discerned faces. At ambient temperatures near $-14 \text{ }^\circ\text{C}$ in a water-drop cloud, the branch tips appear completely rounded except for the leading vertex (e.g., Figure 8). Such a distinct change of shape raises a few questions: Do small prism faces exist on the rounded tips? Is there an abrupt transition between vicinal and round tips? We address these questions in turn.

The question about the existence of leading prism faces on rounded tips might not be definitely answered for a long time; nevertheless, several arguments indicate that the branch tip grows *as if* it had leading prism faces. One, the mechanism described here for the formation of the main rib required prism faces, and the crystal in Figure 8 and other “round tip” crystals show a main rib. Thus, the observed ribs indicate leading prism faces. This argument presumes that no other plausible mechanism exists for rib formation that would also apply to branch tips without leading faces. One cannot rule out that such a mechanism will not be found; however, if such a mechanism existed, then one would expect melt-grown ice dendrites, which have no prism faces, to have a main rib like that on a round-tip snow crystal. But they have no such ribs.⁵⁶ Two, the inferred surface supersaturation of about 0.005 at the tip, based on the measured growth rate at $-14.4 \text{ }^\circ\text{C}$,

slightly exceeds the measured σ_{cr} value of about 0.004 on the prism face, in good agreement with the modeled growth of a snow crystal at this temperature with leading prism faces.²⁸ As the last supporting argument, a plausible mechanism by which the tips would completely round has not yet emerged. Two obvious choices, kinetic roughening and vapor–liquid–solid growth, have the disadvantage that they would require surface supersaturations σ_{ss} that are about 40 and 30 times greater, respectively, than the estimated value.²⁸ Thus, these established “rounding” processes are unlikely to occur; and if they do not occur, it is natural to postulate that the prism faces continually become narrower as the growth rate increases but nevertheless continue to exist.

Such a process of continual face narrowing is a natural extension of the inverse relation between growth rate and branch width described previously. Moreover, a similar process has been observed in experiments on NH_4Br (a cubic crystal) branches growing from solution. In the experiments, Maurer et al.⁵⁷ measured a change from fully vicinal branch tips to fully rounded ones as the growth speed increased. But directly measuring the face area when the tip rounded was difficult, so they used an indirect method that involved fitting a parabola to the tip region and measuring the deviation between the leading vertex and the parabola tip. The results indicated that the faces never completely vanished; rather, the face area slowly shrank and became indistinguishable as the growth rate increased. Use of their method on the tips of the lower sidebranch and branch in Figure 8 resulted in deviations from a parabola of about $7\ \mu\text{m}$ for both cases. As this is roughly the image resolution, the result is inconclusive; however, if better image resolution is achieved, their method may help determine whether leading prism faces exist on the rounded tips of snow crystals. Presently, we only know that the tips grow as if they had prism faces.

Vanishing of Side Vertices. Despite the uncertainty about their leading prism faces, rounded tips such as the one in Figure 8 clearly do not have side vertices. This is consistent with the branches in a 2-D simulation of branch growth.⁵ However, those simulations did not produce side vertices under any conditions,⁵ which suggests that the large vapor sink of the backside of real 3-D crystals might be needed for side vertices to form. A mechanism through which this vapor sink affects the side vertices is described here.

Although the σ -contours, growth rate, and branch size are all closely linked, it is helpful to imagine adjusting the branch width and σ -contours independently. For example, in Figure 5, C is a local σ_s -maximum. However, if the branch width is decreased, the vapor sink becomes weaker; at a small enough width, the local σ_s -maximum at C may vanish, thus making the side vertex a σ_s -minimum. If an SCR forms, it will form at this vertex, effectively removing the side vertex. In this case, there is no macrostep on the leading face, so a new side vertex cannot form during growth. Instead, the SCR position may move closer to the tip, making the leading faces smaller and harder to distinguish.²⁸ Such a change in σ -contours is made clearer by contrasting two limiting cases: a snow crystal consisting solely of six growing hexagonal plates at the ends of nongrowing branches

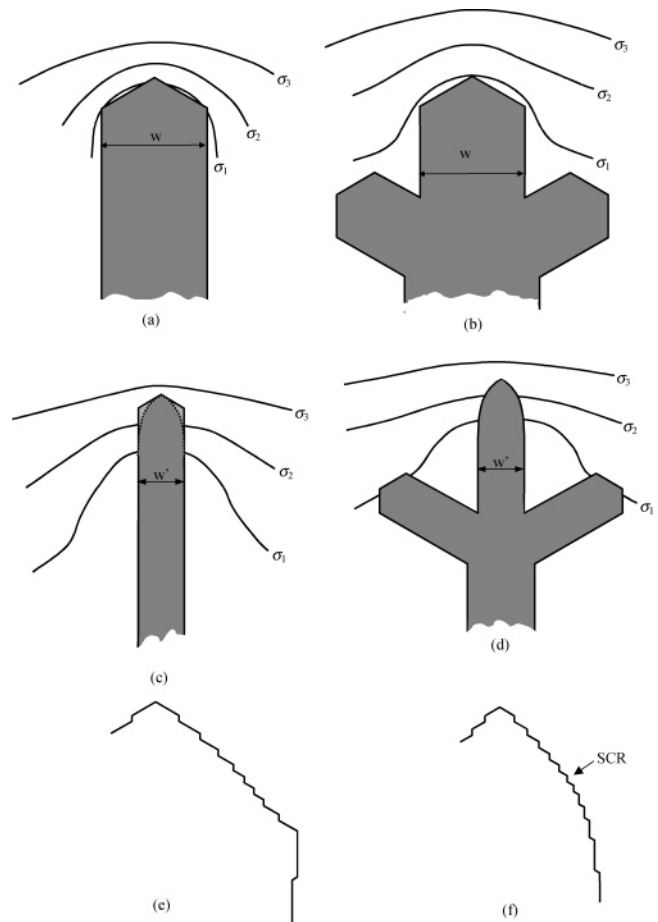


Figure 9. Vanishing of the side vertices on stellar and dendritic crystals. (a) Relatively wide branch of width w with no sidebranches (type P1c). (b) Branch of width w with sidebranches (type P1e). (c) Narrow branch with no sidebranches ($w' < w$) (type P1d). Lighter gray region is the initial tip shape; dotted, dark gray region is the shape after side vertices vanish. The contours are based on those measured in ref 58 for a different material. (d) Narrow branch with sidebranches (P1e or P1f). In (a–d), σ_1 , σ_2 , and σ_3 are vapor supersaturation contours with the same values in all sketches. (e) Step profile on the leading faces for cases (a) and (b) with σ_s -maxima at the side vertices. (f) Step profile on the leading faces for cases (c) and (d) with no σ_s -maximum except at the tip. The relative step heights and separations are enlarged in (e) and (f).

that are joined at a nongrowing crystal center versus the case of six nongrowing branches on a growing central hexagonal plate. In the former case, if the six plates are well separated, the contours will be similar to those around isolated plates (i.e., Figure 3a–c) and thus their side vertices will be σ_s -maxima. But in the latter case, the σ -contours in the crystal plane will look like circles around the crystal center, so the leading faces of the branches will superimpose on circular σ -contours. A simple drawing of concentric circles around a branched crystal shows that the side vertices would be σ_s -minima in this case. Clearly, the contours around more realistic crystal branches will lie between these two limiting cases. This is examined in more detail next.

Consider the three representative σ -contours around the crystal branches in Figure 9. In the wide branch of Figure 9a, contour σ_1 crosses the leading face and side face, thus making σ_s -maxima on the side vertices. This

of the macrostep may be nonprism and some steps might still propagate from D' towards the side vertex. However, once the macrostep is high enough to partly shield region D' from vapor, then the side vertex A'' (which was previously C) will be the source of steps on the face below D . Provided that the regime has sufficiently fast growth, a second macrostep will form somewhere between A'' and the σ_s -minimum point B'' (time t_4). At this time, the side rib changes direction because A'' is now the step source for both adjacent faces. Thus, the side rib starts growing at 60° from the main rib as shown. (Such a feature is seen at e in Figure 1.) At roughly the same time or earlier, a third macrostep should form on the side face at D'' because the supersaturation decreases rapidly along the side face. The net result is that a sidebranch sprouts from the main branch. Also, because the inside corner of the macrostep face at D' is closer to the leading vertex than B (where macrosteps form during constant growth conditions), the process results in a narrower branch above the sidebranch than below. Such a width change is commonly seen in snow crystal images (e.g., d in Figure 1). This width decrease might not always remain because the branch above the sidebranch will subsequently widen more rapidly than that below the sidebranch. Thus, the macrostep model appears capable of explaining sidebranching and related features on dendritic snow crystals.

Sidebranch Density. This sidebranching process is made semiquantitative as follows. Referring to Figure 10 and rearranging the violation condition of eq 2, the condition for a macrostep to form between A'' and B'' is

$$\alpha_s(\sigma_{ss}(A''B''))\sigma_{ss}(A''B'')/\sigma_s(B'') \geq 1 \quad (4)$$

As discussed above, if this condition is met, the same condition is met with B'' replaced by some point D'' on the side face. Therefore, eq 4 is the sidebranching condition. Also, one can view the left side of eq 4 as a step-clumping indicator because step clumping should form when it equals or exceeds unity.²⁸ This equation will now be used to explain why the sidebranch density is typically greater at higher growth rates. Assume that the surface supersaturations at A , B , and C in Figure 10 have the fixed ratios of $1:b:c$, respectively, for example, $1.0:0.9:0.95$. We require only that $1 > c > b$ to ensure that the side vertex is a local σ_s -maximum. As α_s increases rapidly with σ_{ss} above the critical supersaturation σ_{cr} , assume

$$\alpha_s(\sigma_{ss}) = (\sigma_{ss}/\sigma_{cr})^n \quad (5)$$

where $n \gg 1$. Now, consider the situation in which a macrostep is about to form near A . From eq 4, if the growth rate increases, the condition for a macrostep in AB is just reached when

$$(\sigma_s(A)/\sigma_{cr})^n \sigma_s(A)/(b\sigma_s(A)) = 1 \quad (6)$$

where $\sigma_{ss}(AB)$ was set to $\sigma_s(A)$. The question is, if the first macrostep can just form in AB , how close is CB to forming the second macrostep at the same point B ? This is determined using the step-clumping indicator for C . Using $\sigma_{ss}(CB) = c\sigma_{ss}(AB)$ and eq 6, this is

$$(\sigma_s(C)/\sigma_{cr})^n \sigma_s(C)/(b\sigma_s(A)) = c^{n+1} \quad (7)$$

where $\sigma_{ss}(CB)$ was set to $\sigma_s(C)$. This value is closer to 1 for larger values of c . Hence, if the step-clumping indicator at A exceeds 1, it would be more likely for the same to hold for the step-clumping indicator at the side vertex when c is large. Qualitatively, we expect c to be larger for narrow branches than for wide branches because narrow branches have higher supersaturations on their leading face, which require lower supersaturation differences on the face. For example, if $c = 0.95$ for narrow branches and $c = 0.90$ for wide branches, then the ratio of their step-clumping indicators exceeds 3:1 when $n = 20$ (ref 62). Thus, narrow branches can sprout sidebranches more readily than wide branches. Or, given the inverse relation between branch width and growth rate, faster-growing crystals can produce sidebranches more readily than slow-growing crystals. There is another mechanism through which fastest-growing snow crystals in the atmosphere can sprout the most sidebranches. In a typical mixed-phase cloud with significant liquid water content, the data in Table 1 show that a given change of temperature ΔT produces the greatest change in growth rate $\Delta R(AC)$ in the fast-growth regime at temperatures near -14.4°C . Therefore, if temperature fluctuations in the atmosphere are independent of temperature, it will be more likely for a relatively large increase of growth rate to occur at temperatures with fast-growing crystals than it will be at other temperatures. In a real cloud, it is likely that both the larger c and larger $\Delta R(AC)$ contribute to a high sidebranch density. So, not only do the fast-growing crystals have more macrosteps under constant conditions, which we argued causes them to have narrow branches, but the same crystals are more likely to have macrosteps originating from the side vertex leading to sidebranches. This is consistent with the observed correlation between branch width and sidebranch density;⁵⁵ in particular, the highly sidebranched fernlike dendrites (P1f) form in the stellar regime where the branches are narrowest and the growth rate highest.

In the laboratory, both temperature changes and supersaturation changes have produced sidebranching. Experiments in refs 4 and 63 show sidebranch formation when the temperature cycles between -15 and -5°C , and between -15 and -12°C , respectively. But such large values of ΔT are not needed. In the vertical wind tunnel experiments of Takahashi et al.,¹ the temperature of the air stream was kept constant to $\pm 0.4^\circ\text{C}$, yet 1–2 sets of sidebranches formed after 30 min of growth at -14.4°C , whereas no sidebranches formed at other temperatures. However, with conditions constant to $\pm 0.2^\circ\text{C}$ for 10 min, no sidebranches formed. Moreover, temperature fluctuations are not needed; Gonda and Nakahara³ showed that a sudden increase in the ambient supersaturation σ_A would induce sidebranching. Thus, the basic requirement is a change in growth rate, as the macrostep model predicts.

Sidebranch Growth. Sidebranches have unique features due to their growth in an asymmetric vapor density field. A way to see this is sketched in Figure 11. For example, the growth of AB is governed by $\sigma_s(B)$ because $\sigma_s(B) > \sigma_s(A)$ due to B being further from the vapor sink of the branch than A . Initially, when the

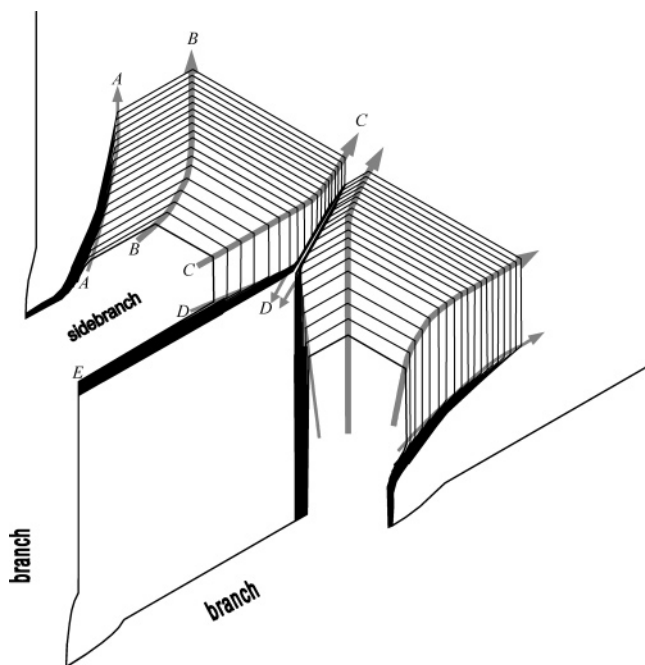


Figure 11. Influence of the nonsymmetric vapor density field on the growth of sidebranches in constant conditions. Gray arrows show the growth directions of the vertices.

sidebranch is small and BC is closer to the branch than it is to the other sidebranch, the growth of BC is governed by $\sigma_s(C)$ because C is furthest from the branch. For the same reason, growth of CD is also governed by $\sigma_s(C)$. Therefore, the main vertex of the sidebranch is initially C and the main vertex strictly follows the straight line at 60° to the branch, producing a straight main rib as shown in Figure 11. But the two leading faces CB and CD do not grow into the same vapor densities. As $\sigma_s(B)$ is initially less than $\sigma_s(C)$, face BC grows faster than AB , thus making the side rib at B have a direction close to that of the main rib at C . Vertex D is both closer to the branch and closer to the crystal center than C , so D has a lower supersaturation than C and probably also B , and thus face DE hardly advances. The consequences are that initially DE is wider than AB , AB is wider than BC , and BC is wider than CD . This is consistent with nearly all sidebranches in Figure 1 (e.g., *f*). However, as the sidebranch grows out away from its main branch and nears the sidebranch of the adjacent branch, $\sigma_s(C)$ decreases, eventually becoming less than $\sigma_s(B)$. Thus, the main vertex shifts to B , and BC , now determined by $\sigma_s(B)$, grows faster than CD . This causes the rib from C to veer upward and the main rib from B to parallel the main branch. Point *j* in Figure 1 shows a similar veering of the main sidebranch rib, presumably due to the changing asymmetries in the vapor density as described above.

Sidebranching on Rounded Branch Tips. Experiments on ice crystals growing with rounded branch tips on a substrate³ found that sidebranches would form only after the growth rate decreased, during which obvious leading faces and side vertices formed, before the growth rate increased. (The growth rate was controlled through the applied supersaturation.) This finding can be understood qualitatively by referring to Figure 12. At time t_1 , the leading face is hard to discern due to both its small size and the absence of side vertices. Then, from

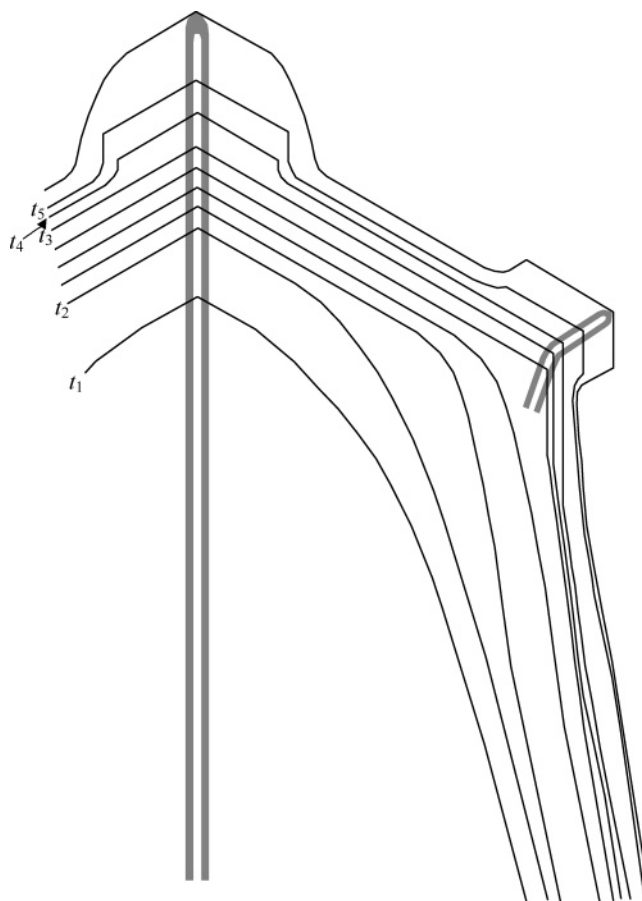


Figure 12. Sidebranch formation on a branch with a rounded tip ($t_1 < t_2 < t_3 < t_4 < t_5$). The growth rate decreases after t_1 and increases after t_3 .

t_2 to t_3 , the growth rate is slower, causing the leading face to increase in size^{5,28} and producing a side vertex. Then, the growth rate increases after t_3 , thus forming macrosteps, first near the main vertex at t_4 , and later at t_5 from the side vertex. As the new tip grows, it again loses its side vertex. This sequence is remarkably similar to the observations in Figure 5 of ref 3. In this way, the macrostep sidebranching mechanism for vicinal tips can be extended to round tips.

In the effectively rough region along the side of the tip, unstable growth due to a local fluctuation, such as a passing drop, could initially promote sidebranching, but the above sidebranching process is expected to remain. The reason is that, even if a bump develops, the tip-most region of the bump will eventually have a prism orientation; once this occurs, the prism face will widen, thus limiting the growth of the bump until a macrostep forms as in the above sidebranching process. Thus, the macrostep sidebranching mechanism would still apply.

In a recent experiment, an applied electric field was used to grow an ice “needle” along an a -axis from a dendrite tip.⁶⁴ When the needle sprouted, the growth rate increased dramatically, the branch width decreased to about $1 \mu\text{m}$, and sidebranching completely ceased. The cause of the high growth rates was explained as an effective increase in the vapor diffusivity, although the lack of sidebranches was not explained. According to the theory proposed here, the lack of sidebranches might be due to a lack of side vertices. Conversely, if

leading faces and side vertices existed at the tip, the extremely small change in σ_s across the face, due to the small width and large vapor diffusivity, may have made it impossible to form the macrosteps needed for side-branching.

Branch Symmetry

It is often stated that the 6-fold symmetry of snow crystals, meaning that each branch has the same length and sidebranch lengths, is a result of each branch growing into the same environmental conditions. This is a necessary condition for symmetry, but it is not sufficient.⁷¹ Another required condition is that each face on the branch has the same response to the local conditions. This requirement is automatically fulfilled by the step-nucleation mechanism but not a dislocation-generated step-source mechanism except in the case that the step density is so high that the surface is effectively rough. In addition, the local conditions depend on the face areas and growth rates (e.g., eq 3). The backsides will have about the same response to local conditions because they are effectively rough, but this is not true for the top faces. Branch-to-branch differences in the top face growth rates might cause differences in the local conditions at the branch tips; moreover, the differences in the top face growth rates might lead to differences in the thicknesses of the prism faces. However, the mass uptake of the top faces are small compared to the backsides, so variations in their growth rates should have little influence on the supersaturation at the tip. Also, if one branch has a slightly faster basal growth rate than the others, the adjacent leading faces would hardly increase in thickness for the following reason. The face thickness is controlled by the position of the SCR where the face bounds the backside, and this position is largely controlled by the local conditions, which would hardly change by the previous argument. Thus, the observed branch symmetry partly owes its existence to the dominant vapor sink on the backsides and the step-nucleation mechanism on the prism faces.

Summary

Established crystal growth ideas have been used here to develop a macrostep model of branch growth on snow crystals. In this model, when macrosteps form on the prism faces, their position and direction determine the characteristics of various observable crystal features. As such, the causes of distinct growth forms including sector plates, broad-branch crystals, stellars, dendrites, and various mixed forms can now be understood at the level of crystal growth surface processes that respond to specific atmospheric conditions. In particular,

- (i) The ribs and grooves, which give each crystal much of its uniqueness, can arise from processes on the leading faces and thus provide important clues about growth on the leading prism faces.
- (ii) The noncrystallographic surface areas account for most of the total mass uptake to the crystal.
- (iii) The leading faces of branches can generate macrosteps under constant growth conditions that lead to narrow branches without sidebranching. Further

analysis suggests that the prism-face growth rate should be inversely related to the branch width, as is observed.

(iv) The side ribs grow at angles of less than 60° to the main rib and change to about 60° when the side vertex becomes the step-source position for both adjacent prism faces. In contrast, the side grooves have angles exceeding 60°.

(v) Branches grow wider at the tip when the growth rate decreases because macrosteps can develop on the side faces without forming on the leading faces.

(vi) A transition from vicinal branch tip to rounded tip may occur on stellar and fernlike dendrites when the side vertices vanish on the narrow branches that form near -14 °C.

(vii) Sidebranches can form on broad-branch crystals, stellars, and dendrites when the growth rate increases sufficiently rapidly due to macrosteps originating from the side vertices. Within limits, the sidebranch density should increase with an increase of the prism-face growth rate.

(viii) The 6-fold symmetry in some branched snow crystals is due to not only uniform environmental conditions but also to the step-nucleation growth mechanism and the dominant vapor sink on the branch backsides.

Several additional comments should also be mentioned here.

A problem that became apparent while writing this paper is the wide variation of meanings for the crystal types “sector plate”, “broad branch”, “stellar”, and “dendrite” in the literature. For example, stellar and broad-branch crystals are often called dendrites, and there is much confusion over the labeling of sectors, broad branches, and stellars. The branch growth processes and interior features, such as those described here, may help to make the existing crystal classification scheme more rigorous.

Meteorological studies of snow crystals have focused on basal and prism faces, although there are reasons that the noncrystallographic regions should also be studied. For example, due to their dominance of the mass uptake, noncrystallographic regions may also have a role in impurity uptake and surface chemical reactions, both topics being important in atmospheric chemistry. Also, the side grooves at the inside corners may promote sidebranch detachment during dendrite evaporation as recent experiments indicate.⁶⁶ This may help explain some cases of “secondary ice crystal production”, a problem of interest for the development of precipitation.

Finally, I address the near symmetry in habit about the fernlike-dendrite regime in the well-known Nakaya habit diagram. It has been assumed that $\alpha_s(\sigma_{ss})$ largely controls the growth rate variations, at least over small temperature changes. This means that the branch width should be inversely related to α_s . Hence, if there is a peak in $\alpha_s(\sigma_{ss})$ versus temperature, there should be habits of the same branch width on both sides of the peak temperature. In this way, the symmetry in the habit diagram follows from the observed growth rate peak in the fernlike dendrite regime near -14 °C. Regarding this peak, the fernlike-dendrite regime was found to extend to -13 °C when the liquid water content

of the cloud increases.⁶⁷ Since $\alpha_s \sim (\sigma_{ss}/\sigma_{cr})^n$, the peak in growth rate near -14 °C, and its extension to -13 °C, are expected to be due to a peak in σ_{ss}/σ_{cr} in this temperature range. This and other predictions from the macrostep model should be tested experimentally. Nevertheless, despite the qualitative and semiquantitative approach, the underlying processes in this model have been justified by the successful predictions of the theory. Thus, with the findings presented here, more detailed numerical studies of snow crystals can be pursued with greater confidence.

Acknowledgment. I thank Charles Knight, Tsuneya Takahashi, and Eric Erbe for the photomicrographs and SEM images. This paper is largely an extension of ideas from Frank's¹⁵ review paper, a seminar by C. Knight at NCAR in 1994, and a relatively obscure conference proceeding by Akira Yamashita.¹⁴ Much help came from discussions of ribs and step sources on snow crystals with C. Knight, who also suggested I use the term "macrostep" instead of Frank's term "lacuna", and also from a critical reading by Marcia Baker. Sci-cubed is the nonprofit organization officially called Science for the Sake of Science.

Appendix: Numerical Simulation of Branch Growth

The assumptions and conditions used in the simulation that produced Figure 7a are as follows: (1) Supersaturation $\sigma(x)$ depended only on the projected position x along the branch axis. Its functional form was fit to σ_A at large x and the estimated supersaturations²⁸ at the tip and the crystal center. (2) The crystal dimension d at time t obeyed the empirical function for crystals at $T = -14.4$ °C from Table 2 of ref 1. (3) The initial branch tip width was $80 \mu\text{m}$ and a new macrostep formed at a new tip width of $56 \mu\text{m}$ whenever the branch tip width reached $80 \mu\text{m}$. (4) The crystal started growth at 600 s with a crystal diameter $2^*d = 1361 \mu\text{m}$ and $w = 80 \mu\text{m}$. The positions of all vertices were then updated every second for 104 s, after which five sets of macrosteps had formed and grown as shown in Figure 7a. More specifically, the functional form of σ was

$$\sigma(x) = (a + \sigma_A x^4)/(b + x^4) \quad (\text{A1})$$

where the ambient supersaturation σ_A is 0.15 (Table 2) and a and b were fit to the calculated supersaturations at the tip ($x = d$) and a supersaturation at the center ($x = 0$) of 0.2 times that at the tip. The σ_s value at the tip σ_{ss} was found by fitting the measured growth rate dd/dt to

$$dd/dt = 1.15\Omega v N_{eq} \sigma_{ss} \alpha_s(\sigma_{ss})/4 \quad (\text{A2})$$

where the volume per molecule in ice Ω is $3.26 \times 10^{-29} \text{ m}^3$, the mean speed of a vapor molecule v is 551 m s^{-1} , the equilibrium vapor density N_{eq} is $4.89 \times 10^{22} \text{ m}^{-3}$, and the factor 1.15 (i.e., $2/3^{1/2}$) is due to the difference in orientation between the branch axis and the leading faces. The α function is that for step nucleation from the derivation⁶⁸ in eqs A3 and A5 of ref 28. In the latter equation, x_s and the face dimension were both set to $1 \mu\text{m}$ and the critical supersaturation σ_{cr} was set to 0.004.

The rates of growth at the vertices were updated every second using a short program in Mathematica 2.2.

As a test of the assumption that growth occurs by step nucleation, I repeated the calculation with the α function appropriate for spiral step growth instead of step nucleation (BCF, with $\sigma_1 = 0.004$). The branch grew very wide, with a rate that was 60% greater than the growth rate of the tip. In contrast, for the step-nucleation case above, the tip grew about 10 times faster than the width. Therefore, it is unlikely that long, narrow branches can grow exclusively by spiral steps.

References

- (1) Takahashi, T.; Endoh, T.; Wakahama, G.; Fukuta, N. *J. Meteorol. Soc. Jpn.* **1991**, *69*, 15.
- (2) Hallett, J.; Knight, C. *Atmos. Res.* **1994**, *32*, 1.
- (3) Gonda, T.; Nakahara, H. *J. Cryst. Growth* **1996**, *173*, 162.
- (4) Libbrecht, K. G. *Eng. Sci.* **2001**, *1*, 10.
- (5) Yokoyama, E.; Kuroda, T. *Phys. Rev. A* **1990**, *41*, 2038.
- (6) Nittmann, J.; Stanley, H. E. *Nature* **1986**, *321*, 663.
- (7) Kobayashi, R. *Physica D* **1993**, *63*, 410.
- (8) Karma, A.; Rappel, W.-J. *Phys. Rev. E* **1998**, *57*, 243.
- (9) Reiter, C. A. *Chaos, Solitons Fractals* **2005**, *23*, 1111.
- (10) Kim, T.; Lin, M. C. Proceedings of ACM SIGGRAPH/Eurographics Symposium on Computer Animation; Breen, D., Lin, M., Eds.; Eurographics Association: Aire-la ville, Switzerland, 2003.
- (11) Uehara, T.; Sekerka, R. F. *J. Cryst. Growth* **2003**, *254*, 251.
- (12) Debierre, J.-M.; Karma, A.; Celestini, F.; Guerin, R. *Phys. Rev. E* **2003**, *68*, 041604.
- (13) Knight, C. A. *Trans. Am. Geophys. Union* **1972**, *53*, 382.
- (14) Yamashita, A. Proceedings of the International Conference on Cloud Physics, Boulder, CO, 1976, American Meteorological Society: Boston, 1976; p 136.
- (15) Frank, F. C. *Contemp. Phys.* **1982**, *23*, 3.
- (16) Nakaya, U. *Snow Crystals, Natural and Artificial*; Harvard University Press: Cambridge, MA, 1954.
- (17) Magono, C.; Lee, C. W. *J. Fac. Sci. Hokkaido Univ. Ser. 7* **1966**, *2*, 321.
- (18) Marshall, J. S.; Langleben, M. P. *J. Meteorol.* **1954**, *11*, 104.
- (19) Lamb, D.; Scott, W. D. *J. Cryst. Growth* **1972**, *12*, 21.
- (20) Hallett, J. *Philos. Mag.* **1961**, *6*, 1073.
- (21) Gonda, T.; Matsuura, Y.; Sei, T. *J. Cryst. Growth* **1994**, *142*, 171.
- (22) Gonda, T.; Sei, T. *Curr. Top. Cryst. Growth Res.* **2002**, *6*, 83.
- (23) Many experiments that indicate surface quasi-liquid are summarized in Petrenko, V. F.; Whitworth, R. W. *Physics of Ice*; Oxford University Press: Oxford, 1999.
- (24) Burton, W. K.; Cabrera, N.; Frank, F. C. *Philos. Trans. R. Soc. London* **1951**, *A243*, 299.
- (25) Mason, B. J.; Bryant, G. W.; Van den Heuvel, A. P. *Philos. Mag.* **1963**, *8*, 505.
- (26) Kuroda, T.; Lacmann, R. *J. Cryst. Growth* **1982**, *56*, 189.
- (27) Mason, B. J. *Proc. R. Soc. London A* **1993**, *441*, 3.
- (28) Nelson, J. *Philos. Mag.* **2001**, *81*, 2337.
- (29) In the linear regime, the growth rate equals that in which all molecules that impinge on the surface can be assumed to grow into the crystal, and the rate of surface evaporation equals that which occurs in equilibrium. When some surface process increases the evaporation flux, the growth rate is less than the linear value (ref 48, eq 3).
- (30) Beckmann, W.; Lacmann, R. *J. Cryst. Growth* **1982**, *58*, 433.
- (31) Sei, T.; Gonda, T. *J. Cryst. Growth* **1989**, *94*, 697.
- (32) Libbrecht, K. G. *J. Cryst. Growth* **2003**, *258*, 168.
- (33) Nelson, J.; Baker, M. B. *J. Geophys. Res.* **1996**, *101*, 7033.
- (34) Equation 3 has been generalized from two face types to an arbitrary number. For rough regions, A_i can be divided into small areas in which each has a nearly uniform R .
- (35) Mizuno, Y. *J. Glaciol.* **1978**, *21*, 409.
- (36) McKnight, C. V.; Hallett, J. *J. Glaciol.* **1978**, *21*, 397.
- (37) Chernov, A. A. *J. Cryst. Growth* **1974**, *24–25*, 11.
- (38) Wood, S.; Baker, M.; Calhoun, D. *J. Geophys. Res.* **2001**, *100*, 4845.
- (39) Levi, L.; Nasello, O. B. *Atmos. Res.* **2003**, *66*, 107.
- (40) Libbrecht, K. G. *J. Cryst. Growth* **2003**, *258*, 168.

- (41) A variation on the dislocation-aided growth mechanism is described in the discussion of Figure 9a in ref 48. Using the BCF step-motion model, it is straightforward to show that the condensation coefficient is roughly equal to $2x_s/p$ for symmetric step capture with p the face perimeter.
- (42) When the molecular mean free path in the air is much smaller than x_s , the growth rate dependence on supersaturation is more complex than the pure-vapor case (Gilmer, G. H.; Ghez, R.; Cabrera, N. *J. Cryst. Growth* **1971**, *8*, 79). The dependence was shown to be roughly quadratic in Nelson, J. Ph.D. Dissertation, University of Washington, Seattle, WA, 1994.
- (43) Lewis, B. *Crystal Growth*; Pamplin, B. R., Ed.; Pergamon Press: Great Britain, 1980; p 23.
- (44) De Yoreo, J. J.; Land, T. A.; Dair, B. *Phys. Rev. Lett.* **1994**, *73*, 838.
- (45) Bacon, N. J.; Baker, M. B.; Swanson, B. D. *Q. J. R. Meteorol. Soc.* **2003**, *129*, 1903.
- (46) Frank, F. C. *J. Cryst. Growth* **1974**, *24/25*, 3.
- (47) Hallett, J. *Am. Sci.* **1984**, *72*, 582.
- (48) Nelson, J.; Knight, C. A. *J. Atmos. Sci.* **1998**, *55*, 1452.
- (49) The sporadic regime at the lowest supersaturations can probably be ruled out for branched snow crystals because it requires that each step spreads across the face before the next one nucleates. With such a process, it would be hard to explain the inferred clumping of steps into macrosteps that occurs symmetrically on all six branches.
- (50) Giga, Y.; Rybka, P. *Adv. Math. Sci. Appl.* **2003**, *13*, 625.
- (51) Also known as Berg's effect.⁵² It follows from eq 3, given the decrease of h_i away from face i .
- (52) Giga, Y.; Rybka, P. *Adv. Math. Sci. Appl. (Gakkotosho, Tokyo)* **2003**, *13*, 625.
- (53) When σ_A decreases or remains low, the pit can instead close up, leaving a void.⁵⁴ Photos of crystals with open pits, sealed-off voids, and combinations of both are on pages 24–49 of ref 55.
- (54) Gonda, T.; Koike, T. *J. Cryst. Growth* **1983**, *65*, 36.
- (55) Bentley, W. A.; Humphreys, W. J. *Snow Crystals*; Dover: New York, 1962.
- (56) Tirmizi, S. H.; Gill, W. N. *J. Cryst. Growth* **1987**, *85*, 488.
- (57) Maurer, J.; Bouissou, P.; Perrin, B.; Tabeling, P. *Europhys. Lett.* **1989**, *8*, 67.
- (58) Emsellem, V.; Tabeling, P. *Europhys. Lett.* **1994**, *25*, 277.
- (59) Lacmann, R.; Stranski, I. N. *J. Cryst. Growth* **1972**, *13/14*, 236.
- (60) Caroli, B.; Muller-Krumbhaar, H. *ISIJ Int.* **1995**, *35*, 1541.
- (61) Another scenario is possible. If the initial surface supersaturation $\sigma_{s1}(C)$ at time t_1 significantly increases to $\sigma_{s2}(C)$ at time t_2 before the steps that left A at t_1 reach C , then it is possible that macrosteps from A and C form nearly simultaneously on the leading face. This can occur because the step spacing y at C has not yet narrowed in response to the shorter steps now emanating from A . With widely spaced steps at C , new steps may nucleate at C at the rate determined by $\sigma_{s2}(C)$ and form a macrostep. It is not clear whether this actually occurs; but it cannot presently be ruled out. Nevertheless, the result is essentially the same as the more likely process sketched in Figure 10.
- (62) From the previously mentioned relation $\alpha_s(\sigma_{ss}) \sim \exp[-48\sigma_{cr}/\sigma_{ss}]$ near $\sigma_{cr}/\sigma_{ss} = 1$, the exponent $n = 48$ at $\sigma_{ss} \approx \sigma_{cr}$ but is somewhat smaller at higher σ_{ss} .
- (63) See <http://www.its.caltech.edu/~atomic/>. Accessed March 1, 2004.
- (64) Libbrecht, K. G.; Tanusheva, V. M. *Phys. Rev. Lett.* **1998**, *81*, 176.
- (65) USDA Agricultural Research Center's Electron Microscopy Unit Snow Page. <http://www.lpsi.barc.usda.gov/emusnow/>. Accessed November 10, 2002.
- (66) From the study reported in Takahashi, T.; Endoh, T. Proceedings of 14th International Conference on Clouds and Precipitation; Bologna, Italy, July 19–23, 2004; Vol. 2, p 936. Later experiments showed severe erosion at the base of sidebranches during crystal evaporation and evidence that the fragile sidebranches sometimes detached (Takahashi, T., personal communication).
- (67) Takahashi, T.; Endoh, T. Proceedings of the 13th International Conference on Clouds and Precipitation; Reno, NV, 2000; p 677.
- (68) Equation A5 in ref 28 has a few typos that are easily corrected by re-deriving it from A3 and A4.
- (69) Hokkaido Education University's Snow Quest web page. <http://yukipro.sap.hokkyodai.ac.jp> (in Japanese). Accessed November 10, 2002.
- (70) This increase was suggested in ref 48 because a larger σ_{cr} value was inferred from a previous experiment at -50 °C. In addition, theory predicts such an increase^{28,38} below -15 °C, and the data in ref 32 suggest such an increase even though the author did not interpret the data in terms of σ_{cr} values. Also, σ_{cr} at an inside corner (e.g., D' in Figure 5) might be lower than that away from a corner, but this has not been studied.
- (71) As a counter-example of the 6-fold symmetric snow crystal, bullet rosettes, in which columnar crystals grow outward from a common center, do not generally have columnar "branches" of the same length and thickness. (See photos in Gow, A. *J. Glaciol.* **1965**, *5*, 461.)

CG049685V